Computation Bits Maximization for IRS-aided Mobile-edge Computing Networks with Phase Errors and Transceiver Hardware Impairments

Sun Mao, Ning Zhang, *Senior Member, IEEE*, Jie Hu, *Senior Member, IEEE*, Kun Yang, *Fellow, IEEE*, Youzhi Xiong, and Xiaosha Chen

***Abstract*—Intelligent reflecting surface (IRS) is a hopeful technique to improve the computation offloading efficiency for mobile-edge computing (MEC) networks. However, the phase errors (PEs) of IRS and transceiver hardware impairments (THIs) will greatly degrade the performance of IRS-assisted MEC networks. To overcome this bottleneck, this paper first investigates the computation bits maximization problem for IRS-assisted MEC networks with PEs, where multiple Internet of Things (IoT) devices can offload their computation tasks to access points with the aid of IRS. By exploiting the block coordinate descent method, we design a multi-block optimization algorithm to tackle the non-convex problem. In particular, the optimal IRS phase shift, time allocation, transmit power and local computing frequencies of IoT devices are derived in closed-form expressions. Moreover, we further study the joint impact of PEs and THIs on the total computation bits of considered systems, where same methods in the scenario with PEs are used to obtain the optimal IRS phase shift and local computing frequencies of IoT devices, while an approximation algorithm and the variable substitution method are used to acquire the optimal transmit power and time allocation strategy. Finally, numerical results validate that our proposed methods can significantly outperform benchmark methods in terms of total computation bits.**

***Index Terms*—Mobile-edge computing, resource management, intelligent reflecting surface, phase errors, transceiver hardware impairments.**

This work is supported in part by the Natural Science Foundation of China under Grants 62241108, 62132004, 61971102 and 62101370, in part by the Natural Science Foundation of Sichuan Province under Grants 2022NSFSC0479 and 2022NSFSC0480, in part by the Sichuan Science and Technology Program under Grants 2022YFH0022 and 22QYCX0168, in part by the UESTC Yangtze Delta Region Research Institute-Quzhou under Grant 2022D031.

Sun Mao is with College of Computer Science, Sichuan Normal University, Chengdu, 610101, China, and also with Visual Computing and Virtual Reality Key Laboratory of Sichuan, Sichuan Normal University, Chengdu, 610101, China, and also with Education Big Data Collaborative Innovation Center of Sichuan 2011, Chengdu, 610101, China. (e-mail: sunmao@sicnu.edu.cn).

Ning Zhang is with Department of Electrical and Computer Engineering, University of Windsor, ON, N9B 3P4, Canada. (e-mail: ning.zhang@ieee.org).

Jie Hu is with School of Information and Communication Engineering, University of Electronic Science and Technology of China, Chengdu, 611731, China. (e-mail: hujie@uestc.edu.cn).

Kun Yang is with School of Information and Communication Engineering, University of Electronic Science and Technology of China, Chengdu, 611731, China, and also with the School of Computer Science and Electronic Engineering, University of Essex, Colchester, CO4 3SQ, U.K. (e-mail: kyang@ieee.org).

Youzhi Xiong is with College of Physics and Electronic Engineering, Sichuan Normal University, Chengdu, 610101, China. (e-mail: yzxiong@sicnu.edu.cn).

Xiaosha Chen is with College of Computer Science and Technology (College of Data Science), Taiyuan University of Technology (TYUT), Taiyuan, 030024, China. (e-mail: pdcxs@outlook.com).

I. Introduction

In recent years, mobile-edge computing (MEC) is envisioned as a crucial technique to meet the stringent performance requirements of emerging computation-intensive and latency-sensitive applications, such as smart cities, industrial internet of things, and so on [1], [2]. MEC leverages edge servers deployed at the access point (AP) to enable mobile devices to offload their computation tasks for parallel computing, thereby reducing computing latency and energy consumption of mobile devices. However, the service quality of MEC is fundamentally restricted by the stochastic wireless propagation environments, particularly when the communication links between the AP and mobile devices are intermittently blocked by some obstacles or experience deep fading [3], [4]. Therefore, it is of importance to improve the performance of MEC networks from the communication perspective.

Benefitted from rapid advancements in digital metamaterials, intelligent reflecting surface (IRS) has emerged as an innovative solution to enhance the spectral-efficiency and energy-efficiency of wireless communications [5]–[9]. An IRS is comprised of massive passive reflection units that can adjust their phases for reshaping the wireless propagation environments. In general, the benefits introduced by IRS mainly include the virtual array gain and reflect beamforming gain, where the former gain is achieved by combining both the direct-link and IRS-aided cascade-link signals, while the latter gain can be realized by optimally configured the phase shifts of reflection elements integrated on IRS. By fully exploiting the two types of gains, IRS has great potential to improve the service quality of MEC, through enhancing the computation offloading efficiency of mobile devices. However, due to the amplification noises and quantization errors, the IRS phase errors and transceiver hardware impairments generally exist in IRS-aided MEC networks, which will lead to the performance degradation of computation offloading. Therefore, this paper focuses on designing the robust computation offloading and reflection optimization strategy for IRS-aided MEC networks, in order to alleviate the negative impact of imperfect hardware on system performance.

A. Related Works

Aiming at harnessing the reflection beamforming gain from the IRS, the existing literature studied a variety of

applications of IRS in wireless communications. In [10], Pan *et al.* leveraged IRS to enhance the information transmission rate of cell-edge users, and they presented a weight sum rate maximization problem that jointly optimized transmit beamforming at the AP and reflect beamforming of the IRS. In [11], Tang *et al.* integrated the IRS with physical-layer security technique to enhance the secrecy rate of legitimate devices in the presence of malicious eavesdroppers. In [12] and [13], the authors used IRS to eliminate harmful co-channel interference in device-to-device communications and downlink non-orthogonal multiple access networks, respectively. The IRS was also applied to enhance the coverage and reliability of mmwave/THz communication systems in [14] and [15]. In addition to improving the transmission efficiency, IRS was also used to overcome the severe path-loss of wireless energy transfer. In [16] and [17], the authors investigated system power consumption minimization and total throughput maximization problems for IRS-empowered wireless powered communication networks, respectively.

The combination of IRS with MEC has also been studied in the literature. In [18], Bai *et al.* first integrated the IRS technique into MEC networks, and studied the resource scheduling for latency minimization. Their subsequent work in [19] focused on realizing sustainable computation services for IRS-aided wireless powered MEC networks, where IRS is deployed to improve the efficiency of uplink task offloading and downlink wireless energy transfer. In [20] and [21], the authors maximized the total computation bits or minimized the system energy consumption for IRS-aided MEC networks. In [22], Hu *et al.* proposed a deep learning-based multi-domain resource scheduling method to eliminate the complex channel estimation process in IRS-aided MEC networks. In [23], Li *et al.* revealed the achievable maximum energy efficiency for IRS-aided MEC networks. Considering the potential information leakage in MEC, our prior work in [24] utilized the IRS to perform the secure task offloading. In addition, Li *et al.* in [25] further presented the artificial noise-enhanced transmission method to avoid the information leakage in IRS-aided MEC networks.

Noted that above works considered an ideal scenario with perfect IRS and transceiver hardware, which is not realistic due to quantization errors, amplification noises, and so forth [26]–[28]. Recently, some research works investigated the IRS-aided wireless communications considering phase errors (PEs) of IRS and transceiver hardware impairments (THIs) of other communication nodes. In [29], Zhou *et al.* studied the secure rate maximization problem for IRS-assisted communication systems in the presence of malicious eavesdroppers and non-ideal THIs. In [30], Xing *et al.* maximized the achievable rate for IRS-aided wireless communication systems considering the impairments in IRS and transceivers. Besides, Chu *et al.* in [31] investigated the impact of PEs and THIs on wireless information and energy transmissions, and they further proposed throughput maximization-based resource scheduling method. Our previous article in [32] focused on revealing the minimum transmission time for IRS-aided full-duplex wireless powered communication networking considering PEs of IRS.

TABLE I: Brief comparison of related literature

Ref.	Optimization target	IRS	MEC	PEs	HWIs
[18]	Computation latency	✓	✓	✗	✗
[19] [20] [22]	Total computation bits	✓	✓	✗	✗
[21]	System energy consumption	✓	✓	✗	✗
[23]	Computation efficiency	✓	✓	✗	✗
[24]	Secure energy consumption	✓	✓	✗	✗
[25]	Secure computation efficiency	✓	✓	✗	✗
[29]	Secure transmission rate	✓	✗	✗	✓
[30] [31]	Achievable transmission rate	✓	✗	✓	✓
[32]	Total transmission time	✓	✗	✓	✗
This paper	Total computation bits	✓	✓	✓	✓

TABLE I summarizes the key elements of aforementioned literature. As observed, previous works on IRS-aided MEC networks studied the joint transmit power control, IRS phase shift matrix, communication and computation resources optimization method considering perfect hardware, which can help enhance the performance of computation latency [18], total computation bits [19], [20], [22], energy efficiency [21], [23], and security [24], [25]. However, due to the existence of PEs and THIs [29]–[32], such a joint resource management and reflection optimization design is no longer optimal and may lead to severe performance degradation for IRS-aided MEC networks. First, the stochastic PEs will incur the derivation of reflect beamforming, and it will further degrade the performance of computation offloading. In addition, due to the existence of IRS, the noise signal introduced by THIs tends to be enlarged to influence the computation offloading. Therefore, it is essential to design joint resource management and reflection optimization method in the presence of PEs and THI. However, the imperfect hardware and coupled optimization variables (such as transmit power and phase shift matrix, etc.) will make the joint optimization problem strictly non-convex and NP-hard. To this end, it is important but challenging problem to design low-complexity resource management and reflection optimization algorithm for IRS-aided MEC networks considering PEs and THIs, which motivates this article.

B. Novelty and Contribution

To this end, this paper examines the impact of PEs and THIs on the performance of a typical IRS-aided MEC networks, where IoT devices can offload part of their computation-intensive tasks to the AP with the aid of IRS. Furthermore, we investigate the joint resource management and reflection optimization method to maximize the total computation bits, which is a direct performance metric to measure the computing capability of IRS-aided MEC networks. The main contribution of this paper is outlined as follows:

- *New design framework for IRS-aided MEC with imperfect hardware:* Different from existing literature considering perfect hardware, this paper develops an optimal design framework for IRS-aided MEC networks taking into account of IRS phase errors and transceiver

hardware impairments. Particularly, the PE of each reflection element at the IRS is modelled as a random variable that follows an uniform distribution at the interval $[-\pi/2, \pi/2]$, and the transceiver hardware impairments of AP and IoT devices are modelled as the additive Gaussian noise associated with the signal power.

- *Computation bits maximization for the scenario with PE:* We formulate a computation bits maximization problem with phase errors, subject to the phase shift constraints of IRS, the stochastic phase error constraints, and the maximum energy consumption, transmit power, and local computing frequency constraints of IoT devices. To handle this strictly non-convex problem, we utilize the block coordinate descent method to develop a multi-block optimization method. For the phase shift optimization subproblem, different from conventional semi-definite relaxation method with high computational complexity, we first transform the stochastic phase errors into a deterministic form, and further adopt the successive convex approximate method to obtain the optimal phase shift of IRS in closed-form expressions. For the local computing frequency optimization subproblem, we derive the optimal solution in closed-form expressions by exploiting the feature of optimization problem. For the transmit power and time allocation subproblem, some auxiliary variables are introduced to convert it into a convex problem, and then we use the Lagrange duality method and Karush-Kuhn-Tucker (KKT) conditions to acquire the optimal solution in closed-form expressions.
- *Computation bits maximization for the scenario with PE and THI:* We further reveal the impact of both PEs and THIs on the total accomplished computation bits of considered systems. In addition, the optimal IRS phase shifts and local computing frequencies of IoT devices are obtained using similar methods adopted in the previous scenario. Moreover, we develop an iterative algorithm to obtain the optimal transmit power and time allocation strategy using variable substitution and approximation methods.

Numerical results are provided to evaluate the performance of the proposed methods. It is shown that our methods significantly outperform several benchmark methods, including without IRS scheme, random phase shift scheme, full offloading scheme, and local computing only scheme. This demonstrates that the optimal design of IRS phase shift has great potential to improve the total accomplished computation bits, and the partial offloading strategy can fully exploit both the local and edge computing capabilities. Furthermore, our proposed method exhibits lower total computation bits than that of the ideal scenario without PEs and THIs, which further verifies that the PEs and THIs have a negative impact on the performance of IRS-aided MEC networks.

The remainder of this paper is summarized as follows. Section II presents the system model. Section III investigates the computation bits maximization problem with IRS phase errors. In Section IV, we further reveal the impact of both phase errors and transceiver hardware impairments on the total computation bits for considered systems. Section V provides simulation results to evaluate the performance of our proposed schemes. Conclusions are presented in Section VI.

II. System Model

As shown in Fig. 1 (a), this paper focuses on a typical IRS-aided MEC network comprised by an AP integrated with edge servers, K IoT devices indexed by $\mathcal{K} = \{1, 2, \cdots, K\}$, and an IRS with M reflection units indexed by $\mathcal{M} = \{1, 2, \cdots, M\}$. Each IoT device needs to execute the computation task via local computing and task offloading to the AP. Moreover, an IRS is equipped to enhance the computation offloading of IoT devices. Specifically, we consider a practical scenario with hardware impairments of IRS and other communication nodes, due to the quantization errors, amplification noises, and so on [27], [28], which will degrade the performance of considered systems.

Noted that our considered system can be found in practical applications. Taking a wireless camera for example, such IoT devices are deployed to execute particular monitor tasks, e.g., object detection, environmental surveillance, etc. To achieve the real-time video analysis, the wireless cameras equipped with central processing unit (CPU) chips can execute a part of computation tasks locally, and offload the rest of computation tasks to nearby AP with the aid of IRS.

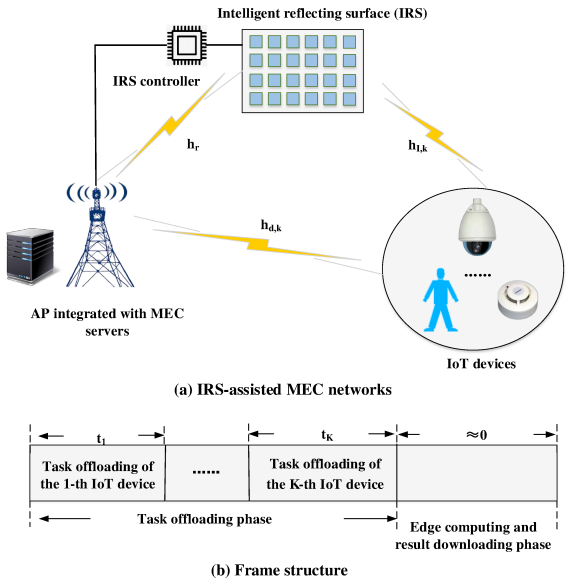

Fig. 1: System model.

A. Channel Model

This work adopts a block-based channel model where channels remain fixed at the current frame but may change at the boundaries of time frames. We define $h_{d,k}$, $\mathbf{h}_{I,k} \in \mathbb{C}^{M\times 1}$ and $\mathbf{h}_r^H \in \mathbb{C}^{1\times M}$ as the channel from the k-th IoT device to the AP, from the k-th IoT device to the IRS, and from the IRS to the AP, respectively. Similar to [19], [33], all the

channel state information can be perfectly acquired by the AP, in order to reveal the limit performance for considered systems. Noted that we can measure the direct channels between the AP and IoT devices by setting the IRS into absorbing state. Additionally, the cascade channels between the IRS and AP/IoT devices can be estimated by installing a small number of low-power sensors at the IRS.

B. Local Computing

Defining f_k as the CPU-cycle frequency of k-th IoT device, the amount of accomplished computation bits via local computing will be

$$D_{l,k} = \frac{f_k T}{C_k}, \forall k \in \mathcal{K}, \tag{1}$$

where C_k represents the number of CPU cycles required for executing 1-bit task, T denotes the duration of time frame. According to [34], the power consumption of k-th IoT device for local computing is expressed as $P_{l,k} = \kappa f_k^3, \forall k \in \mathcal{K}$, where κ denotes an effective capacitance coefficient associated with the CPU architecture [35], [36]. Hence, the computation energy consumption of k-th IoT device is given by

$$E_{l,k} = P_{l,k} T = \kappa T f_k^3, \forall k \in \mathcal{K}. \tag{2}$$

C. Task Offloading

Except for local computing, each IoT device tends to offload its computation-intensive task to the AP with the help of IRS. As illustrated in Fig. 1(b), a time division multiple access (TDMA) protocol is employed to support multi-user task offloading. In the time slot t_k, the k-th IoT device sends its computation task to the AP with the aid of IRS. This paper investigates two scenarios: one with PE only and the other with both PE and THI. We first analyze the impact of PE on the total computation performance of considered systems in Section III, and then examine the impact of both PE and THI in Section IV.

1) Task Offloading with PE only: In the case with phase errors only, the signal received at the AP during t_k is expressed as

$$y_k^{\text{PE}} = (h_{d,k} + \mathbf{h}_r^H \Gamma_k \mathbf{h}_{I,k}) \sqrt{P_k} s_k + n_k, \forall k \in \mathcal{K}, \tag{3}$$

where P_k and s_k denote the transmit power and signal symbol of k-th IoT device, respectively, $n_k \sim \mathcal{CN}(0, \delta^2)$ stands for the Gaussian noise signal with δ^2 being the noise power. During the t_k time slot, the actual phase shift matrix of the IRS is represented by $\Gamma_k = \text{diag}\{e^{j(\theta_{k,1}+\theta_{E,k,1})}, e^{j(\theta_{k,2}+\theta_{E,k,2})}, \cdots, e^{j(\theta_{k,M}+\theta_{E,k,M})}\}$, where $\theta_{k,m}$ and $\theta_{E,k,m}$ represent the phase shift and the additive random phase error of the m-th reflection unit during t_k, respectively. Similar to [31], the phase shift error follows the uniform distribution, i.e., $\theta_{E,k,m} \sim \mathcal{U}(-\frac{\pi}{2}, \frac{\pi}{2})$. As a result, the bits of offloaded task by the k-th IoT device is given by

$$R_k^{\text{PE}} = t_k B \log_2 \left(1 + \frac{P_k |h_{d,k} + \mathbf{h}_r^H \Gamma_k \mathbf{h}_{I,k}|^2}{\delta^2}\right), \forall k \in \mathcal{K}, \tag{4}$$

where B denotes the system bandwidth.

2) Task Offloading with PE and THI: In the case with both PE and THI, the signal received at the AP is expressed as

$$y_k = (h_{d,k} + \mathbf{h}_r^H \Gamma_k \mathbf{h}_{I,k})(\sqrt{P_k} s_k + \epsilon_{t,k}) + \epsilon_{r,k} + n_k, \forall k \in \mathcal{K}, \tag{5}$$

where $\epsilon_{t,k} \sim \mathcal{CN}(0, \delta_t P_k)$ and $\epsilon_{r,k} \sim \mathcal{CN}(0, \delta_r P_k |h_{d,k} + \mathbf{h}_r^H \Gamma_k \mathbf{h}_{I,k}|^2)$ represents the random transceiver hardware impairments at the k-th IoT device and the AP during t_k [30], [37], respectively. Hence, the amount of offloaded computation bits by the k-th IoT device is given by

$$R_k = t_k B \log_2 \left(1 + \frac{P_k |h_{d,k} + \mathbf{h}_r^H \Gamma_k \mathbf{h}_{I,k}|^2}{P_k(\delta_r + \delta_t)|h_{d,k} + \mathbf{h}_r^H \Gamma_k \mathbf{h}_{I,k}|^2 + \delta^2}\right), \forall k \in \mathcal{K}. \tag{6}$$

The communication energy consumption of k-th IoT device is expressed as

$$E_{c,k} = P_k t_k, \forall k \in \mathcal{K}. \tag{7}$$

After receiving the computing tasks from IoT devices, the AP needs to process the received tasks and transmit the computation results back to IoT devices. This paper concentrating on revealing the impact of PEs and THIs on the achievable total computation bits of IRS-aided MEC networks. Due to powerful computation capability and abundant communication resources at the AP [1], it is reasonable to ignore the time cost for data processing at edge server and result downloading [22], [23].

III. Computation Bits Maximization for IRS-assisted MEC With Phase Errors

This section studies the influence of phase errors on the performance of IRS-aided MEC networks. We aim at maximizing the total accomplished computation bits through jointly optimizing the phase shift matrix $\{\Gamma_k, \forall k \in \mathcal{K}\}$ of IRS, time allocation $\{t_k, \forall k \in \mathcal{K}\}$, transmit power $\{P_k, \forall k \in \mathcal{K}\}$ and CPU frequencies $\{f_k, \forall k \in \mathcal{K}\}$ of IoT devices, which can be formulated as

$$\underset{\{\Gamma_k, f_k, t_k, P_k\}}{\text{maximize}} \sum_{k=1}^{K} \left(t_k B \log_2 \left(1 + \frac{P_k |h_{d,k} + \mathbf{h}_r^H \Gamma_k \mathbf{h}_{I,k}|^2}{\delta^2}\right) + \frac{f_k T}{C_k}\right) \tag{8a}$$

$$\text{s.t.} \quad E_{l,k} + E_{c,k} \le E_{k,\max}, \forall k \in \mathcal{K}, \tag{8b}$$

$$\sum_{k=1}^{K} t_k \le T, \tag{8c}$$

$$0 \le \theta_{k,m} \le 2\pi, \forall k \in \mathcal{K}, \forall m \in \mathcal{M}, \tag{8d}$$

$$0 \le P_k \le P_{k,\max}, \forall k \in \mathcal{K}, \tag{8e}$$

$$0 \le f_k \le f_{k,\max}, \forall k \in \mathcal{K}, \tag{8f}$$

$$t_k \ge 0, \forall k \in \mathcal{K}, \tag{8g}$$

[1]In the scenario with massive number of IoT devices, the limited edge resources will be the main design bottleneck for IRS-aided MEC networks. It is promising to investigate the multi-layer MEC framework [38], [39], and it is out of the scope of this article.

where $E_{k,\max}$, $P_{k,\max}$ and $f_{k,\max}$ denote the maximum available energy consumption, maximum transmit power, and maximum CPU-cycle frequency of k-th IoT device, respectively, (8b) represents the maximum energy consumption constraints of IoT devices, (8c) implies that the total task offloading duration of IoT devices cannot exceed the time frame length, (8d) is the phase shift constraint of IRS, (8e) and (8f) restricts the maximum transmission power and CPU frequencies of IoT devices, respectively.

Remark 1: The problem (8) of maximizing computation bits is strictly non-convex due to the coupled optimization variables such as transmit power P_k and time allocation t_k, and phase shift matrix Γ_k and transmit power P_k, as well as the stochastic phase errors of IRS.

Therefore, this paper utilizes the block coordinate descent method to address the non-convex problem (8) through alternately solving the following three subproblems, including phase shift optimization subproblem, local computing frequency optimization subproblem, and transmit power and time allocation subproblem. For the phase shift optimization subproblem, we convert the stochastic phase errors into a deterministic form, and use the successive convex approximation technique to acquire the optimal phase shift matrix of IRS, which can be expressed using closed-form equations. Additionally, the optimal local computing frequencies of IoT devices are also deduced in closed-from expressions according to the problem structure. For the transmit power and time allocation subproblem, we exploit the variable substitution technique to transform it into a convex problem, and obtain the optimal solution in closed-form expressions using the Lagrange duality method and KKT conditions. The flowchart to solve (8) is illustrated in Fig. 2.

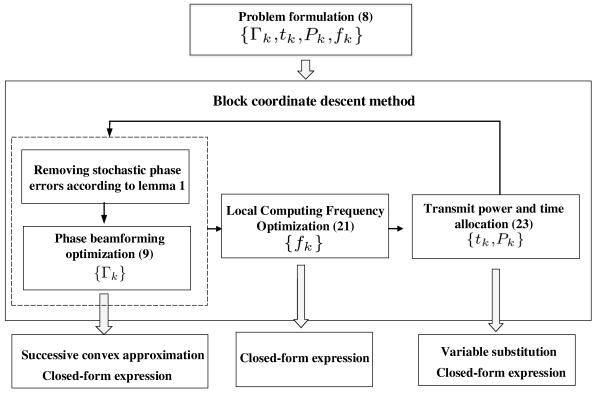

Fig. 2: The flowchart to solve (8).

A. Phase Beamforming Optimization Subproblem

For given $\{t_k^*, P_k^*, f_k^*\}$, (8) is converted to the phase beamforming optimization subproblem. Since R_k^{PE} increases with $|h_{d,k} + \mathbf{h}_r^H \Gamma_k \mathbf{h}_{I,k}|^2$, so the phase beamforming optimization subproblem is equivalent to

$$\underset{\{\Gamma_k\}}{\text{maximize}} \sum_{k=1}^{K} |h_{d,k} + \mathbf{h}_r^H \Gamma_k \mathbf{h}_{I,k}|^2 \tag{9a}$$

$$\text{s.t.} \quad \text{(8d), (8g).} \tag{9b}$$

Since $\Gamma_k = \hat{\Gamma}_{E,k} \hat{\Gamma}_k$ where $\hat{\Gamma}_k = \text{diag}\{e^{j\theta_{k,1}}, e^{j\theta_{k,2}}, \cdots, e^{j\theta_{k,M}}\}$ and $\hat{\Gamma}_{E,k} = \text{diag}\{e^{j\theta_{E,k,1}}, e^{j\theta_{E,k,2}}, \cdots, e^{j\theta_{E,k,M}}\}$, it follows that

$$\begin{aligned} a_k &= |\mathbf{h}_r^H \Gamma_k \mathbf{h}_{I,k} + h_{d,k}|^2 = |\mathbf{h}_r^H \hat{\Gamma}_{E,k} \hat{\Gamma}_k \mathbf{h}_{I,k} + h_{d,k}|^2 \\ &= |\mathbf{v}_{E,k}^T \text{diag}(\mathbf{h}_r^H) \text{diag}(\mathbf{h}_{I,k}) \mathbf{v}_k + h_{d,k}|^2 = |\mathbf{v}_{E,k}^T \mathbf{A}_k^H \mathbf{v}_k + h_{d,k}|^2 \\ &= (\mathbf{v}_{E,k}^T \mathbf{A}_k^H \mathbf{v}_k + h_{d,k})^H (\mathbf{v}_{E,k}^T \mathbf{A}_k^H \mathbf{v}_k + h_{d,k}) \\ &= \mathbf{v}_k^H \mathbf{A}_k \text{conj}(\mathbf{v}_{E,k}) \mathbf{v}_{E,k}^T \mathbf{A}_k^H \mathbf{v}_k + \mathbf{v}_k^H \mathbf{A}_k \text{conj}(\mathbf{v}_{E,k}) h_{d,k} \\ &+ h_{d,k}^H \mathbf{v}_{E,k}^T \mathbf{A}_k^H \mathbf{v}_k + h_{d,k}^H h_{d,k}, \forall k \in \mathcal{K}. \end{aligned} \tag{10}$$

In (10), $\mathbf{v}_k = [e^{j\theta_{k,1}}, \cdots, e^{j\theta_{k,M}}]^T$, $\mathbf{v}_{E,k} = [e^{j\theta_{E,k,1}}, \cdots, e^{j\theta_{E,k,M}}]^T$, and $\mathbf{A}_k = \text{diag}(\mathbf{h}_{I,k}^H) \text{diag}(\mathbf{h}_r)$. Introducing (10) into (9), we can reformulate the phase shift optimization subproblem as

$$\underset{\{\mathbf{v}_k\}}{\text{maximize}} \sum_{k=1}^{K} \mathbb{E}_{\mathbf{v}_{E,k}}(a_k) \tag{11a}$$

$$\text{s.t.} \quad \text{(8d), (8g).} \tag{11b}$$

It should be noted that the expectation of $\sum_{k=1}^{K} a_k$ is maximized to remove the randomness of phase errors. Additionally, *Lemma 1* is derived to simplify the objective function (11a).

Lemma 1: $\mathbb{E}_{\mathbf{v}_{E,k}}(a_k)$ can be converted into

$$\begin{aligned} \hat{a}_k &= \mathbb{E}_{\mathbf{v}_{E,k}}(a_k) \\ &= h_{d,k}^H h_{d,k} + \mathbf{v}_k^H \mathbf{A}_k \mathbb{E}_{\mathbf{v}_{E,k}} \left(\text{conj}(\mathbf{v}_{E,k}) \mathbf{v}_{E,k}^T \right) \mathbf{A}_k^H \mathbf{v}_k + \\ &\mathbf{v}_k^H \mathbf{A}_k \mathbb{E}_{\mathbf{v}_{E,k}}(\text{conj}(\mathbf{v}_{E,k})) h_{d,k} + h_{d,k}^H \mathbb{E}_{\mathbf{v}_{E,k}}(\mathbf{v}_{E,k}^T) \mathbf{A}_k^H \mathbf{v}_k \\ &= h_{d,k}^H h_{d,k} + \mathbf{v}_k^H \mathbf{A}_k \mathbf{R} \mathbf{A}_k^H \mathbf{v}_k + \frac{2}{\pi} \mathbf{v}_k^H \mathbf{A}_k \mathbf{1} h_{d,k} + \\ &\frac{2}{\pi} h_{d,k}^H \mathbf{1}^T \mathbf{A}_k^H \mathbf{v}_k, \forall k \in \mathcal{K}, \end{aligned} \tag{12}$$

where

$$\mathbf{R} = \begin{bmatrix} 1 & \frac{4}{\pi^2} & \cdots & \frac{4}{\pi^2} \\ \frac{4}{\pi^2} & 1 & \cdots & \frac{4}{\pi^2} \\ \vdots & \vdots & \ddots & \vdots \\ \frac{4}{\pi^2} & \frac{4}{\pi^2} & \cdots & 1 \end{bmatrix}_{M \times M}. \tag{13}$$

Proof: Please refer to Appendix A. ■

Utilizing *Lemma 1*, (11) is expressed as

$$\underset{\{\mathbf{v}_k\}}{\text{maximize}} \sum_{k=1}^{K} \hat{a}_k \tag{14a}$$

$$\text{s.t.} \quad \text{(8d).} \tag{14b}$$

After some matrix transformations, (14) is reformulated as

$$\underset{\{\hat{\mathbf{v}}_k\}}{\text{maximize}} \sum_{k=1}^{K} \hat{\mathbf{v}}_k^H \mathbf{Q}_k \hat{\mathbf{v}}_k \tag{15a}$$

$$\text{s.t.} \ |\hat{\mathbf{v}}_k(m)| = 1, \forall k \in \mathcal{K}, \forall m \in \{\mathcal{M}, M+1\}, \tag{15b}$$

where $\hat{\mathbf{v}}_k = [\mathbf{v}_k^T, 1]^T$,

$$\mathbf{Q}_k = \begin{bmatrix} \mathbf{A}_k \mathbf{R} \mathbf{A}_k^H & \frac{2}{\pi}\mathbf{A}_k \mathbf{1} h_{d,k} \\ \frac{2}{\pi}(\mathbf{A}_k \mathbf{1} h_{d,k})^H & h_{d,k}^H h_{d,k} \end{bmatrix}. \tag{16}$$

As observed, (15a) and (15b) can be decomposed for individual $\hat{\mathbf{v}}_k$. Hence, the optimal $\hat{\mathbf{v}}_k$ is obtained by addressing K subproblems as follows.

$$\underset{\hat{\mathbf{v}}_k}{\text{maximize}} \ \hat{\mathbf{v}}_k^H \mathbf{Q}_k \hat{\mathbf{v}}_k \tag{17a}$$

$$\text{s.t.} \ |\hat{\mathbf{v}}_k(m)| = 1, \forall m \in \{\mathcal{M}, M+1\}. \tag{17b}$$

Since (17a) is non-concave, the SCA method can be utilized to tackle it. According to the convex optimization theory, (17a) should satisfy the following inequalities

$$\hat{\mathbf{v}}_k^H \mathbf{Q}_k \hat{\mathbf{v}}_k \leq (\hat{\mathbf{v}}_k^{(i)})^H \mathbf{Q}_k \hat{\mathbf{v}}_k^{(i)} + 2\text{Re}\{(\hat{\mathbf{v}}_k^H - (\hat{\mathbf{v}}_k^{(i)})^H)\mathbf{Q}_k \hat{\mathbf{v}}_k^{(i)}\} \tag{18}$$

where $\hat{\mathbf{v}}_k^{(i)}$ denotes the local optimal solution at the i-th iteration. Therefore, (17) is transformed to solve the following problem at the i-th iteration until convergence.

$$\underset{\hat{\mathbf{v}}_k}{\text{maximize}} \ \text{Re}\{\hat{\mathbf{v}}_k^H \mathbf{Q}_k \hat{\mathbf{v}}_k^{(i)}\} \tag{19a}$$

$$\text{s.t.} \ |\hat{\mathbf{v}}_k(m)| = 1, \forall m \in \{\mathcal{M}, M+1\}. \tag{19b}$$

To maximize (19a), the optimal solution of (19) should satisfy

$$\hat{\mathbf{v}_k}^* = \exp(-j\text{arg}(\mathbf{Q}_k \hat{\mathbf{v}}_k^{(i)})). \tag{20}$$

To sum up, the proposed method to solve (9) is detailed in Algorithm 1.

Algorithm 1: Successive convex approximation-based algorithm to solve phase shift optimization subproblem (9)

1 **Initialize:** Setting $\{\mathbf{v}_k^{(0)}\}$, and iteration factor $i = 1$.
2 **Repeat:**
3 Calculating optimal $\{\hat{\mathbf{v}}_k^*\}$ according to (20) for given $\{\hat{\mathbf{v}}_k^{(i)} = [(\mathbf{v}_k^{(i)})^T, 1]^T\}$;
4 Obtaining $\{\mathbf{v}_k^*\}$ from $\{\hat{\mathbf{v}_k^*}\}$;
5 Updating $\{\mathbf{v}_k^{(i+1)} = \mathbf{v}_k^*\}$ and iteration index $i = i + 1$;
6 **Until** convergence.
7 **Returning** optimal solution $\{\mathbf{v}_k^*\}$.

B. Local Computing Frequency Optimization Subproblem

Given $\{\Gamma_k^*, P_k^*, t_k^*\}$, (8) is reduced to the local computing frequency optimization subproblem, which is formulated as

$$\underset{\{f_k\}}{\text{maximize}} \ \sum_{k=1}^{K} \frac{f_k T}{C_k} \tag{21a}$$

$$\text{s.t.} \quad \kappa T f_k^3 + P_k^* t_k^* \leq E_{k,\max}, \forall k \in \mathcal{K}, \tag{21b}$$

$$0 \leq f_k \leq f_{k,\max}, \forall k \in \mathcal{K}. \tag{21c}$$

As observed, (21a) increases with the local computing frequencies of IoT devices. Therefore, the IoT devices can adopt the maximum CPU frequency to execute their computation tasks, and the optimal local computing frequency for problem (21) is expressed as

$$f_k^* = \min\left\{f_{k,\max}, \sqrt[3]{\frac{E_{k,\max} - P_k^* t_k^*}{\kappa T}}\right\}, \forall k \in \mathcal{K}. \tag{22}$$

C. Transmit Power and Time Allocation Subproblem

Under given $\{\Gamma_k^*, f_k^*\}$, (8) is simplified as the transmit power and time allocation subproblem

$$\underset{\{t_k, P_k\}}{\text{maximize}} \ \sum_{k=1}^{K} t_k B \log_2\left(1 + \frac{P_k |h_{d,k} + \mathbf{h}_r^H \Gamma_k^* \mathbf{h}_{I,k}|^2}{\delta^2}\right) \tag{23a}$$

$$\text{s.t.} \quad \kappa T (f_k^*)^3 + P_k t_k \leq E_{k,\max}, \forall k \in \mathcal{K}, \tag{23b}$$

$$\sum_{k=1}^{K} t_k \leq T, \tag{23c}$$

$$0 \leq P_k \leq P_{k,\max}, \forall k \in \mathcal{K}, \tag{23d}$$

$$t_k \geq 0, \forall k \in \mathcal{K}. \tag{23e}$$

Introducing the auxiliary variables $E_k = t_k P_k, \forall k \in \mathcal{K}$, (23) is converted to

$$\underset{\{t_k, E_k\}}{\text{maximize}} \ \sum_{k=1}^{K} t_k B \log_2\left(1 + \frac{E_k |h_{d,k} + \mathbf{h}_r^H \Gamma_k^* \mathbf{h}_{I,k}|^2}{t_k \delta^2}\right) \tag{24a}$$

$$\text{s.t.} \quad \kappa T (f_k^*)^3 + E_k \leq E_{k,\max}, \forall k \in \mathcal{K}, \tag{24b}$$

$$0 \leq E_k \leq t_k P_{k,\max}, \forall k \in \mathcal{K}, \tag{24c}$$

$$\text{(23c), (23e).} \tag{24d}$$

Theorem 1: The problem (24) is convex.

Proof: Based on the concave function property [40], we can derive that the logarithmic function $B \log_2\left(1 + \frac{E_k |h_{d,k} + \mathbf{h}_r^H \Gamma_k^* \mathbf{h}_{I,k}|^2}{\delta^2}\right)$ is concave associated with E_k. Therefore, its perspective function $t_k B \log_2\left(1 + \frac{E_k |h_{d,k} + \mathbf{h}_r^H \Gamma_k^* \mathbf{h}_{I,k}|^2}{t_k \delta^2}\right)$ with $t_k > 0$ is also joint concave function related to $\{E_k, t_k\}$. Hence, the objective function (24a) is concave. Together with other linear constraints, (24) is proved as a convex problem. ■

Next, we aim at obtaining the closed-form expressions for the optimal transmit power and time allocation strategy by utilizing the Lagrange duality method and KKT conditions. The partial Lagrange function of (24) is expressed as

$$\begin{aligned} \mathcal{L} = &- \sum_{k=1}^{K} t_k B \log_2\left(1 + \frac{E_k |h_{d,k} + \mathbf{h}_r^H \Gamma_k^* \mathbf{h}_{I,k}|^2}{t_k \delta^2}\right) + \\ &\sum_{k=1}^{K} \lambda_{1,k} (\kappa T (f_k^*)^3 + E_k - E_{k,\max}) + \\ &\sum_{k=1}^{K} \lambda_{2,k} (E_k - t_k P_{k,\max}) + \lambda_3 (\sum_{k=1}^{K} t_k - T) \end{aligned} \tag{25}$$

where $\lambda_{1,k}$, $\lambda_{2,k}$ and λ_3 stand for the non-negative Lagrange multipliers related to (24b)-(24d).

Theorem 2: The optimal transmit power is expressed as

$$P_k^* = \frac{E_k^*}{t_k^*} = \left[\frac{B}{(\lambda_{1,k}+\lambda_{2,k})\ln 2} - \frac{\delta^2}{|h_{d,k}+\mathbf{h}_r^H\Gamma_k^*\mathbf{h}_{I,k}|^2}\right]^+, \forall k \in \mathcal{K}. \tag{26}$$

Proof: The partial derivative of Lagrange function $\mathcal{L}$ to E_k can be derived as

$$\frac{\partial L}{\partial E_k} = -\frac{t_k B}{\ln 2}\frac{\frac{|h_{d,k}+\mathbf{h}_r^H\Gamma_k^*\mathbf{h}_{I,k}|^2}{t_k\delta^2}}{1+\frac{E_k|h_{d,k}+\mathbf{h}_r^H\Gamma_k^*\mathbf{h}_{I,k}|^2}{t_k\delta^2}} + \lambda_{1,k}+\lambda_{2,k}, \forall k \in \mathcal{K}. \tag{27}$$

Letting $\frac{\partial L}{\partial E_k} = 0$, $\forall k \in \mathcal{K}$, the optimal transmit power will be obtained as given in (26). ∎

Remark 2: As seen from (26), the optimal transmit power increases with the transmission bandwidth B and the composite channel gain $|h_{d,k}+\mathbf{h}_r^H\Gamma_k^*\mathbf{h}_{I,k}|^2$. Therefore, IoT devices will utilize more energy to offload their computation tasks to the edge server located at AP when the transmission bandwidth and composite channel gain are large.

Theorem 3: The optimal solution of (24) is realized by exhausting all the available time duration, namely $\sum_{k=1}^{K} t_k^* = T$.

Proof: Theorem 3 will be proved by contradiction. It is assumed that $\{t_k^*, E_k^*\}$ is the optimal solution of (24), and it satisfies $\sum_{k=1}^{K} t_k^* < T$. Besides, the optimal objective function is represented as $R_{\text{tot}}(t_k^*, E_k^*)$. Next, we can construct another feasible solution $\{\zeta t_k^*, E_k^*\}$ where $\zeta = \frac{T}{\sum_{k=1}^{K} t_k^*} > 1$ such that $\sum_{k=1}^{K} \zeta t_k^* = T$, and it can achieve the optimal solution $R_{\text{tot}}(\zeta t_k^*, E_k^*)$. Clearly, $R_{\text{tot}}(t_k^*, E_k^*) < R_{\text{tot}}(\zeta t_k^*, E_k^*)$, because the offloading computation bits increases with the time duration. It contradicts with our assumption, and *Theorem 3* is thus proved. ∎

Lemma 2: $f(x) = \ln(1+x) - \frac{x}{1+x}$ is a monotonic increasing function associated with $x \geq 0$. It exists an unique solution to satisfy $f(x) = J$, and the solution is expressed as $x = -(1 + \frac{1}{\mathcal{W}(-\exp(-(J+1)))})$, where $\mathcal{W}(\cdot)$ denotes the Lambert function.

Proof: Please refer to *Lemma 1* in [41] for detailed proof. ∎

Theorem 4: The optimal time allocation strategy is expressed as

$$t_k^* = -\frac{E_k^*|h_{d,k}+\mathbf{h}_r^H\Gamma_k^*\mathbf{h}_{I,k}|^2}{\delta^2\left(1+\frac{1}{\mathcal{W}\left(-\exp\left(-(\frac{(\lambda_3-\lambda_{2,k}P_{k,\max})\ln 2}{B}+1)\right)\right)}\right)}, \forall k \in \mathcal{K}. \tag{28}$$

Proof: The partial derivative of Lagrange function $\mathcal{L}$ to t_k is given by

$$\frac{\partial L}{\partial t_k} = -\frac{B}{\ln 2}(\ln\left(1+\frac{E_k|h_{d,k}+\mathbf{h}_r^H\Gamma_k^*\mathbf{h}_{I,k}|^2}{t_k\delta^2}\right) - \frac{\frac{E_k|h_{d,k}+\mathbf{h}_r^H\Gamma_k^*\mathbf{h}_{I,k}|^2}{t_k\delta^2}}{1+\frac{E_k|h_{d,k}+\mathbf{h}_r^H\Gamma_k^*\mathbf{h}_{I,k}|^2}{t_k\delta^2}}) - \lambda_{2,k}P_{k,\max} + \lambda_3, \forall k \in \mathcal{K}. \tag{29}$$

By letting $\frac{\partial L}{\partial t_k} = 0$, $\forall k \in \mathcal{K}$, we can derive that

$$\ln\left(1+\frac{E_k|h_{d,k}+\mathbf{h}_r^H\Gamma_k^*\mathbf{h}_{I,k}|^2}{t_k\delta^2}\right) - \frac{\frac{E_k|h_{d,k}+\mathbf{h}_r^H\Gamma_k^*\mathbf{h}_{I,k}|^2}{t_k\delta^2}}{1+\frac{E_k|h_{d,k}+\mathbf{h}_r^H\Gamma_k^*\mathbf{h}_{I,k}|^2}{t_k\delta^2}} = \frac{(\lambda_3-\lambda_{2,k}P_{k,\max})\ln 2}{B}, \forall k \in \mathcal{K}. \tag{30}$$

According to *lemma 2*, by introducing $x = \frac{E_k|h_{d,k}+\mathbf{h}_r^H\Gamma_k^*\mathbf{h}_{I,k}|^2}{t_k\delta^2}$, we have

$$\frac{E_k|h_{d,k}+\mathbf{h}_r^H\Gamma_k^*\mathbf{h}_{I,k}|^2}{t_k\delta^2} = -\left(1+\frac{1}{\mathcal{W}\left(-\exp\left(-(\frac{(\lambda_3-\lambda_{2,k}P_{k,\max})\ln 2}{B}+1)\right)\right)}\right), \forall k \in \mathcal{K}. \tag{31}$$

After some basic transformations, we can derive the optimal time allocation strategy as given in (28). ∎

D. Convergence and Computational Complexity

As described above, the alternating optimization method is proposed to solve the computation bits maximization problem (8). The detailed procedure is illustrated in Algorithm 2.

Algorithm 2: Block coordinate descent-based method for computation bits maximization problem (8) with phase errors

1 **Initialize:** Setting $(t_k^{(0)}, E_k^{(0)}, f_k^{(0)}, \mathbf{v}_k^{(0)})$, and $n = 1$.
2 **Repeat:**
3 Executing Algorithm 1 to acquire the optimal phase shift vector $\{\mathbf{v}_k^{(n)}\}$,
4 Obtaining the optimal local computing frequencies $\{f_k^{(n)}\}$ via (22);
5 Acquiring the optimal transmit energy and time allocation strategy $\{t_k^{(n)}, E_k^{(n)}\}$ by solving (24);
6 Updating iteration coefficient $n = n+1$;
7 **Until** convergence.
8 **Return:** $(t_k^*, P_k^*, f_k^*, \mathbf{v}_k^*)$=$(t_k^{(n)}, \frac{E_k^{(n)}}{t_k^{(n)}}, f_k^{(n)}, \mathbf{v}_k^{(n)})$.

Theorem 5: Algorithm 2 is able to converge to the optimal solution in a finite number of iterations.

Proof: Let $\mathbf{v}_k^{(n)}$, $t_k^{(n)}$, $P_k^{(n)}$ and $f_k^{(n)}$ denote the optimal solution at the n-th iteration. Moreover, the objective function is indicated by $D_{\text{tot}}(\mathbf{v}_k^{(n)}, t_k^{(n)}, P_k^{(n)}, f_k^{(n)})$. In step 3 of Algorithm 2, the optimal phase shift of IRS is acquired for given $t_k^{(n)}$, $P_k^{(n)}$ and $f_k^{(n)}$, which gives

$$D_{\text{tot}}(\mathbf{v}_k^{(n)}, t_k^{(n)}, P_k^{(n)}, f_k^{(n)}) \leq D_{\text{tot}}(\mathbf{v}_k^{(n+1)}, t_k^{(n)}, P_k^{(n)}, f_k^{(n)}). \tag{32}$$

In the step 4, the optimal local computing frequencies are obtained when $\mathbf{v}_k^{(n+1)}$, $t_k^{(n)}$ and $P_k^{(n)}$ are fixed, and it follows that

$$D_{\text{tot}}(\mathbf{v}_k^{(n+1)}, t_k^{(n)}, P_k^{(n)}, f_k^{(n)}) \leq D_{\text{tot}}(\mathbf{v}_k^{(n+1)}, t_k^{(n)}, P_k^{(n)}, f_k^{(n+1)}). \tag{33}$$

In the step 5, the optimal transmit power and time allocation scheme is achieved when $\mathbf{v}_k^{(n+1)}$ and $f_k^{(n+1)}$ are fixed. Hence, we have

$$D_{\text{tot}}(\mathbf{v}_k^{(n+1)}, t_k^{(n)}, P_k^{(n)}, f_k^{(n+1)}) \leq D_{\text{tot}}(\mathbf{v}_k^{(n+1)}, t_k^{(n+1)}, P_k^{(n+1)}, f_k^{(n+1)}). \tag{34}$$

According to above descriptions, we have

$$D_{\text{tot}}(\mathbf{v}_k^{(n)}, t_k^{(n)}, P_k^{(n)}, f_k^{(n)}) \leq D_{\text{tot}}(\mathbf{v}_k^{(n+1)}, t_k^{(n+1)}, P_k^{(n+1)}, f_k^{(n+1)}). \tag{35}$$

Therefore, the objective function of (8) is non-decreasing associated with the iteration index. Besides, due to the maximum energy consumption constraints of IoT devices, the value of total computation bits is limited. Hence, Algorithm 2 can reach to an optimal solution after several iterations. ■

Next, the computational complexity of Algorithm 2 is presented as follows. Let us denote N_1 and N_2 as the iteration number of Algorithm 1 and 2, respectively. The computational complexity for solving (9), (21) and (23) will be

- To solve (9), Algorithm 1 is adopted to obtain the optimal phase shift matrix of IRS. In each iteration of Algorithm 1, we acquire the optimal phase shift of IRS according to (20) with a computational complexity of $\mathcal{O}(K)$. Combined with the iteration number N_1, the total complexity of Algorithm 1 is $\mathcal{O}(N_1 K)$.
- For the local computing frequency optimization subproblem (21), we derive its closed-form solution in (22) with a computational complexity of $\mathcal{O}(K)$.
- To tackle (23), interior point method-based method is used to acquire its optimal solution with $2K$ variables and $3K+1$ constraints, thus the computational complexity is expressed as $\mathcal{O}(4(5K+1)K^2\sqrt{3K+1}\log(\frac{1}{\epsilon_1}))$, where ϵ_1 represents the tolerance factor.

Overall, the total complexity of Algorithm 2 can be expressed as $\mathcal{O}(N_2((N_1+1)K + 4(5K+1)K^2\sqrt{3K+1}\log(\frac{1}{\epsilon_2})))$.

IV. Computation Bits Maximization for IRS-assisted MEC With Phase Errors and Transceiver Hardware Impairments

This section further investigates the joint impact of phase errors and transceiver hardware impairments on the achievable total computation bits of IRS-aided MEC networks. The corresponding optimization problem is expressed as

$$\underset{\{\Gamma_k, t_k, P_k, f_k\}}{\text{maximize}} \sum_{k=1}^{K} (t_k B \log_2\left(1 + \frac{P_k|h_{d,k} + \mathbf{h}_r^H \Gamma_k \mathbf{h}_{I,k}|^2}{P_k(\delta_r+\delta_t)|h_{d,k} + \mathbf{h}_r^H \Gamma_k \mathbf{h}_{I,k}|^2 + \delta^2}\right) + \frac{f_k T}{C_k}) \tag{36a}$$

$$\text{s.t.} \quad E_{l,k} + E_{c,k} \leq E_{k,\max}, \forall k \in \mathcal{K}, \tag{36b}$$

$$\sum_{k=1}^{K} t_k \leq T, \tag{36c}$$

$$0 \leq \theta_{k,m} \leq 2\pi, \forall m \in \mathcal{M}, \forall k \in \mathcal{K}, \tag{36d}$$

$$0 \leq P_k \leq P_{k,\max}, \forall k \in \mathcal{K}, \tag{36e}$$

$$0 \leq f_k \leq f_{k,\max}, \forall k \in \mathcal{K}, \tag{36f}$$

$$t_k \geq 0, \forall k \in \mathcal{K}. \tag{36g}$$

Problem (36) is inherently non-convex owing to several reasons such as stochastic phase errors, interference signals resulting from transceiver hardware impairments, and coupled optimization variables. In order to tackle this problem, we employ the block coordinate descent method to decompose (36) into three subproblems: the IRS phase shift optimization subproblem, the local computing frequency optimization subproblem, and the transmit power and time allocation subproblem. Fig. 3 shows the flowchart for solving (36).

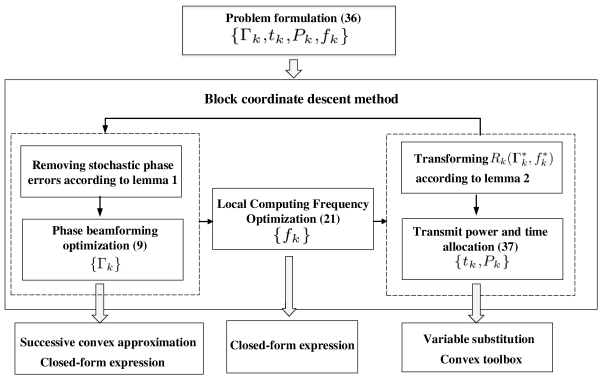

Fig. 3: The flowchart for solving (36).

As seen from Fig. 3, since $\frac{P_k|h_{d,k}+\mathbf{h}_r^H\Gamma_k\mathbf{h}_{I,k}|^2}{P_k(\delta_r+\delta_t)|h_{d,k}+\mathbf{h}_r^H\Gamma_k\mathbf{h}_{I,k}|^2+\delta^2}$ increases with $|h_{d,k} + \mathbf{h}_r^H\Gamma_k\mathbf{h}_{I,k}|^2$, the phase bemforming optimization subproblem is solved by exploiting the same methods proposed in Section III. Meanwhile, the optimal CPU-cycle frequencies of IoT devices are also derived at (22) in Section III. Additionally, we use the variable substitution method and an approximation technique to acquire the optimal transmit power and time allocation strategy.

Given $\{\Gamma_k^*, f_k^*\}$, (36) is reduced to the transmit power and time allocation subproblem

$$\underset{\{t_k, P_k\}}{\text{maximize}} \sum_{k=1}^{K} t_k B \log_2\left(1 + \frac{P_k|h_k|^2}{P_k(\delta_r+\delta_t)|h_k|^2 + \delta^2}\right) \tag{37a}$$

$$\text{s.t.} \quad \kappa T (f_k^*)^3 + P_k t_k \leq E_{k,\max}, \forall k \in \mathcal{K}, \tag{37b}$$

$$\sum_{k=1}^{K} t_k \leq T, \tag{37c}$$

$$0 \leq P_k \leq P_{k,\max}, \forall k \in \mathcal{K}, \tag{37d}$$

$$t_k \geq 0, \forall k \in \mathcal{K}, \tag{37e}$$

where $h_k = h_{d,k} + \mathbf{h}_r^H \Gamma_k^* \mathbf{h}_{I,k}, \forall k \in \mathcal{K}$. As observed, the objective function (37a) is non-convex and non-concave due to the interference signal introduced by transceiver hardware impairments. To tackle it, we utilize the following lemma to transform (37a) to a tractable form.

Lemma 3: Denoting $f(b) = -ba + \ln(b) + 1$, it follows that

$$-\ln a = \max_{y>0} f(b). \tag{38}$$

Noted that the equality holds when $b = 1/a$. Defining $a = P_k|h_k|^2(\delta_r + \delta_t) + \delta^2$ and $b = y_k^{(i)}$, we have

$$R_k(\Gamma_k^*, f_k^*) = t_k B \log_2\left(1 + \frac{P_k|h_k|^2}{P_k(\delta_r+\delta_t)|h_k|^2 + \delta^2}\right) = t_k B \log_2(P_k|h_k|^2(1+\delta_r+\delta_t)+\delta^2) - t_k B \log_2(P_k|h_k|^2(\delta_r+\delta_t) + \delta^2) = t_k B \log_2(P_k|h_k|^2(1+\delta_r+\delta_t)+\delta^2) - \frac{t_k B}{\ln 2}\ln(P_k|h_k|^2(\delta_r+\delta_t)+\delta^2) = t_k B \log_2(P_k|h_k|^2(1+\delta_r+\delta_t) + \delta^2) + \frac{t_k B}{\ln 2}(-y_k^{(i)}(P_k|h_k|^2(\delta_r+\delta_t)+\delta^2) + \ln(y_k^{(i)}) + 1). \tag{39}$$

Introducing (39) into (37), and considering the variable substitution $E_k = P_k t_k, \forall k \in \mathcal{K}$, we can obtain the optimal solution of (37) by iteratively solving the following convex problem

$$\underset{\{t_k, E_k\}}{\text{maximize}} \quad \sum_{k=1}^{K}(t_k B \log_2(\frac{E_k|h_k|^2(1+\delta_r+\delta_t)}{t_k} + \delta^2) + \frac{B}{\ln 2}(-y_k^{(i)}(E_k|h_k|^2(\delta_r+\delta_t)+t_k\delta^2) + t_k(\ln(y_k^{(i)})+1))) \tag{40a}$$

$$\text{s.t.} \quad \kappa T (f_k^*)^3 + E_k \le E_{k,\max}, \forall k \in \mathcal{K}, \tag{40b}$$

$$\sum_{k=1}^{K} t_k \le T, \tag{40c}$$

$$0 \le E_k \le t_k P_{k,\max}, \forall k \in \mathcal{K}, \tag{40d}$$

$$t_k \ge 0, \forall k \in \mathcal{K}. \tag{40e}$$

The detailed procedure for solving the transmit power and time allocation problem (37) is illustrated in Algorithm 3.

Algorithm 3: Proposed method to solve the transmit power and time allocation subproblem (37)

1 **Initialize:** Setting $\{t_k^{(0)}, E_k^{(0)} = P_k^{(0)} t_k^{(0)}\}$, and $i = 1$.
2 **Repeat:**
3 Calculating $y_k^{(i)} = \frac{1}{\frac{E_k^{(i-1)}}{t_k^{(i-1)}}(\delta_t+\delta_r)|h_k|^2+\delta^2}$;
4 Obtaining the optimal $\{t_k^{(i)}, E_k^{(i)}\}$ by solving (40);
5 Updating iteration factor $i = i + 1$;
6 **Until** convergence.
7 **Returning** optimal solution $\{t_k^*, P_k^* = \frac{E_k^*}{t_k^*}\}$.

A. Covergence and Computational Complexity

According to above description, the computation bits maximization problem (36) with both PE and THI can be solved by the following Algorithm 4.

Theorem 6: Algorithm 4 can converge to the optimal solution within finite iterations.

Proof: The proof is similar to *Theorem 5*. ■

According to the algorithm procedure, the computational complexity of Algorithm 4 is presented as follows. Defining

Algorithm 4: Alternating optimization method for solving computation bits maximization problem (33) with phase errors and transceiver hardware impairments

1 **Initialize:** Setting $(t_k^{(0)}, P_k^{(0)}, f_k^{(0)}, \mathbf{v}_k^{(0)})$, and $n = 1$.
2 **Repeat:**
3 Executing Algorithm 1 to acquire the optimal phase shift vector $\{\mathbf{v}_k^{(n)}\}$,
4 Obtaining the optimal local computing frequencies $\{f_k^{(n)}\}$ via (20);
5 Adopting Algorithm 3 to achieve the optimal transmission power and time allocation $\{t_k^{(n)}, P_k^{(n)}\}$;
6 Updating iteration index $n = n + 1$;
7 **Until** convergence.
8 **Return:** $(t_k^*, P_k^*, f_k^*, \mathbf{v}_k^*)$=$(t_k^{(n)}, P_k^{(n)}, f_k^{(n)}, \mathbf{v}_k^{(n)})$.

N_3 and N_4 as the required iteration number of Algorithm 3 and 4, respectively. In each iteration of Algorithm 4, the same methods in Algorithm 2 are adopted to solve the IRS phase shift optimization subproblem and the local computing frequency optimization subproblem, while the corresponding complexity is analyzed in Section III. Besides, Algorithm 3 is utilized to acquire the optimal solution of transmit power and time allocation subproblem (37). The computational complexity of each iteration of Algorithm 3 is $\mathcal{O}(4(5K+1)K^2\sqrt{(3K+1)}\log(\frac{1}{\epsilon_2}))$ using the interior point method-based solver [42]. Therefore, the total computational complexity for solving (37) is given by $\mathcal{O}(4N_3(5K+1)K^2\sqrt{(3K+1)}\log(\frac{1}{\epsilon_2}))$. In summary, we obtain the total computational complexity of Algorithm 4 as $\mathcal{O}(N_4((N_1+1)K + 4N_3(5K+1)K^2\sqrt{(3K+1)}\log(\frac{1}{\epsilon_1})))$.

V. Numerical Results

In this section, we present extensive numerical results that reveal the performance of our proposed methods for IRS-aided MEC networks with phase errors and transceiver hardware impairments, as compared to the following benchmark methods.

- *Without IRS:* In this method, the IoT devices offload their computation tasks to the AP without the assistance of IRS. Considering hardware impairments of AP and IoT devices, the time allocation, transmit power, and local computing frequencies of IoT devices are jointly optimized to maximize the total computation bits.
- *Random phase shift:* In this scheme, the phase shift of IRS is selected from $(0, 2\pi]$ in a random manner. Moreover, the transmit power, time allocation, and local computing frequencies of IoT devices are jointly optimized to maximize the total computation bits.
- *Full offloading scheme:* In this scheme, the IoT devices cannot utilize local computing capability to complete their computation tasks. Except for the local computing frequencies of IoT devices, other variables can be optimized by utilizing the proposed method. Meanwhile, the phase errors of IRS and transceiver hardware impairments are also considered in this method.

- *Local computing only:* In this scheme, the IoT devices only can execute their computation tasks locally, and the AP do not provide the edge computing service for IoT devices.
- *Without PE and THI:* This method considers an ideal scenario without phase errors and transceiver hardware impairments. Thus, it can be envisioned as an upper bound for the proposed methods.

We model the channel coefficient in simulations as

$$\mathbf{C_c} = \sqrt{P_l d^{-\alpha}}\left(\sqrt{\frac{M_r}{M_r+1}}\mathbf{C}^{\text{LoS}} + \sqrt{\frac{1}{M_r+1}}\mathbf{C}^{\text{NLoS}}\right), \quad (41)$$

where d denotes the actual distance between transmit and receive nodes, $\alpha = 2$ stands for the path-loss factor, $P_l = 10^{-2}$ is the path loss of unit distance, $M_r = 4$ indicates the Rician coefficient, and $\mathbf{C}^{\text{LoS}}$ and $\mathbf{C}^{\text{NLoS}}$ are the line-of-sight and Rayleigh fading components, respectively. Moreover, the coordinates of AP, IRS, and IoT devices are located at [0,0,10] m, [-1,5,5] m, and ([1,5,0], [2,4,0]) m, respectively. The other network parameters are set as follows: $K = 2$, $M = 60$, $\kappa = 10^{-28}$, $\delta^2 = 10^{-9}$ W, and $\delta_r = \delta_t = 10^{-5}$. For ease of reference, the simulation parameters are summarized at TABLE II.

TABLE II: Simulation Parameters

Parameter	Value
Computational complexity of task at k-th IoT device, C_k	500
Effective capacitance coefficient related to IoT devices' CPU, κ	10^{-28} [43]
Gaussian noise power, δ^2	10^{-9} W
Maximum transmission power of k-th IoT device, $P_{k,\max}$	0.5 W
Maximum CPU-cycle frequency of k-th IoT device, $f_{k,\max}$	1 GHz
Maximum energy consumption of k-th IoT device, $E_{k,\max}$	0.1 Joule
Number of IoT devices, K	2
Number of reflection units on IRS, M	60
Path-loss coefficient, α	2
Path loss of unit distance, P_l	10^{-2}
Parameter related to the transceiver hardware impairments, δ_r/δ_t	10^{-5} [31]
Rician factor, M_r	4
Transmission bandwidth, B	1 MHz
Time block length, T	1 Seconds

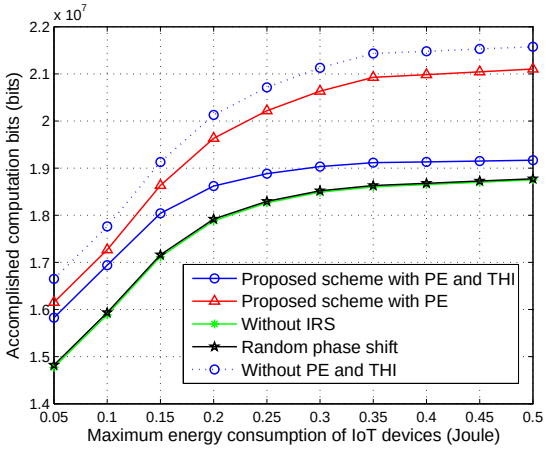

Fig. 4: Total computation bits versus maximum energy consumption of IoT devices.

Figure 4 displays the relationship between the total computation bits and the maximum energy consumption $E_{k,\max}$ of IoT devices, where the maximum local computing frequency of IoT devices is set as $f_{k,\max} = 1$ GHz, the maximum transmit power of IoT devices is $P_{k,\max} = 0.5$ W, the transmission bandwidth is $B = 1$ MHz, the computational complexity is set as $C_k = 500$, and the time frame length is $T = 1$ seconds. We observe that the total computation bits increases with $E_{k,\max}$, and the growth rate of all curves slows down as $E_{k,\max}$ becomes sufficiently large. As $E_{k,\max}$ increases, the IoT devices have more available energy to execute a larger amount of computation bits via local computing and task offloading. Meanwhile, the total accomplished computation bits will be restricted by an upper bound due to the limitations of the maximum transmit power $P_{k,\max}$ and the maximum computing frequencies $f_{k,\max}$ of IoT devices. Therefore, the growth rate of total computation bits slows down as the maximum energy consumption of IoT devices increases. Furthermore, we also see that our proposed methods highly outperform the benchmark schemes (except for the method without PE and THI). This observation demonstrates that the optimal design of IRS phase shift has great potential to improve the total accomplished computation bits, and the hardware impairments of IRS and transceivers impose a negative impact on the total accomplished computation bits.

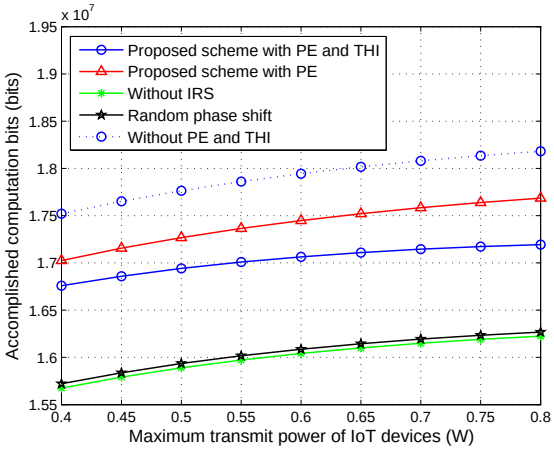

Fig. 5: Total computation bits versus maximum transmit power of IoT devices.

In Fig. 5, the total computation bits are plotted against the maximum transmit power $P_{k,\max}$ of IoT devices, where $f_{k,\max} = 1$ GHz, $E_{k,\max} = 0.1$ Joule, $B = 1$ MHz, $T = 1$ seconds, and $C_k = 500$. As observed, the total computation bits increases with $P_{k,\max}$. This is because that the offloaded computation bits increases with $P_{k,\max}$, and it will further lead to the improvement of total accomplished computation bits. Additionally, our proposed methods outperform both the *Random phase shift* scheme and the *Without IRS* scheme significantly. In addition, we also observe that the proposed method with PE can achieve higher total computation bits compared with the proposed method with PE and THI, and the performance gap between them increases with the maximum transmit power of IoT devices. The reason is that transceiver

hardware impairments lead to the inevitable reduction of total computation bits, and the negative impact will be enlarged with the increase of maximum transmit power of IoT devices.

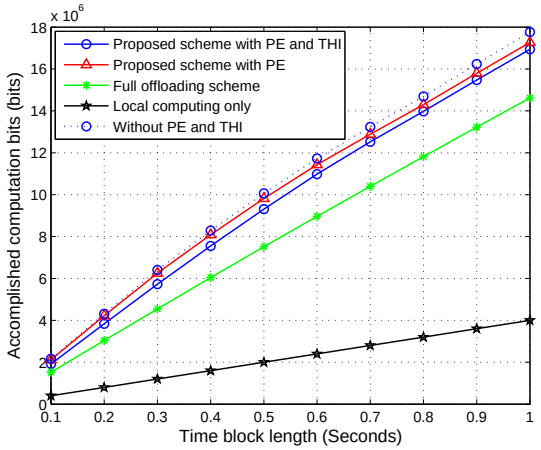

Fig. 6: Total computation bits versus time frame length.

Fig. 6 reveals the total computation bits achieved by different methods against the time block length T, where $f_{k,\max} = 1$ GHz, $E_{k,\max} = 0.1$ Joule, $P_{k,\max} = 0.5$ W, $B = 1$ MHz, and $C_k = 500$. It is seen from this figure that the total accomplished computation bits increases with T. Moreover, the proposed method that considers partial offloading achieves remarkably higher total computation bits than the *Local computing only* scheme and the *Full offloading* scheme, respectively. Because the partial offloading strategy can utilize both the local and edge computing capabilities, while the *Full offloading* scheme and *Local computing only* scheme are envisioned as the special cases of proposed method, e.g., our proposed method is reduced to the *Full offloading* scheme when we set $\{f_k = 0, \forall k \in \mathcal{K}\}$.

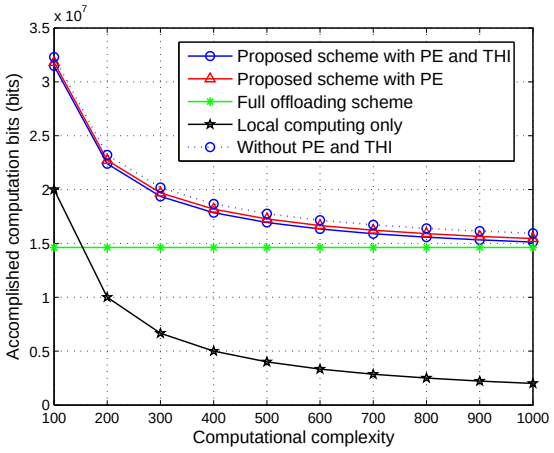

Fig. 7: Total computation bits versus computational complexity.

Fig. 7 shows the total computation bits versus the computational complexity C_k of tasks arrived at IoT devices, where $f_{k,\max} = 1$ GHz, $E_{k,\max} = 0.1$ Joule, $P_{k,\max} = 0.5$ W, $B = 1$ MHz, and $T = 1$ Seconds. As observed, we find that the performance gap between the proposed method and the *Local computing only* scheme increases with the computational complexity C_k. Because, when the computational complexity is sufficiently high, the local computing mode will be inefficient, and it becomes more beneficial to offload more computation-intensive tasks to the edge server with powerful computing capability.

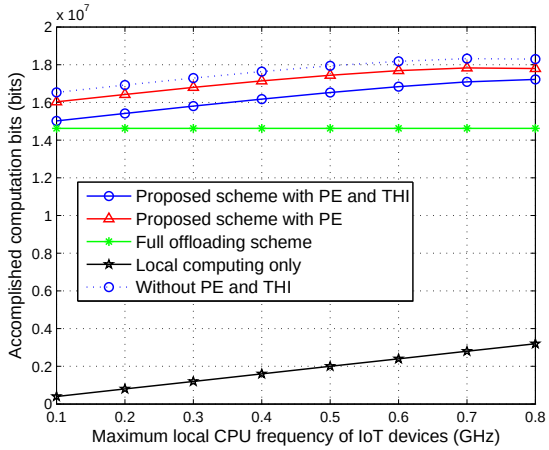

Fig. 8: Total computation bits versus maximum local CPU frequency of IoT devices.

Fig. 8 shows the total computation bits against the maximum local CPU frequency $f_{k,\max}$ of IoT devices, where $E_{k,\max} = 0.1$ Joule, $P_{k,\max} = 0.5$ W, $B = 1$ MHz, $T = 1$ Seconds, and $C_k = 500$. Compared with the *Full offloading* scheme, the performance gain achieved by our proposed method is shown to increase rapidly with the maximum local CPU frequency of IoT devices when $f_{k,\max} \leq 0.6$ GHz, and the growth trend will be slow when $f_{k,\max} > 0.6$ GHz. This is because that the IoT devices will execute a larger amount of computation bits via local CPU with the increase of $f_{k,\max}$, and the total computation bits improved by the proposed method is restricted by the limited energy supply of IoT devices.

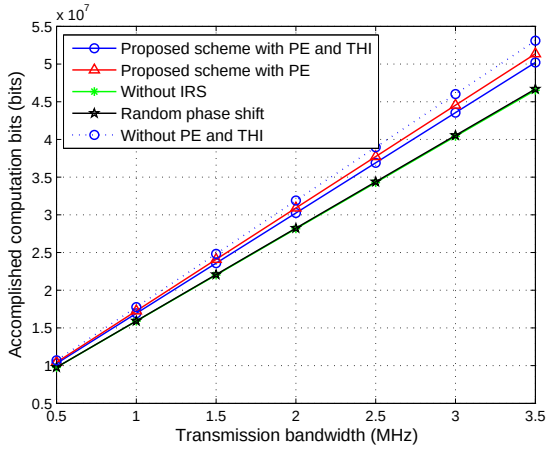

Fig. 9: Total computation bits versus transmission bandwidth.

In Fig. 9, we plot the total computation bits versus the transmission bandwidth B, where $E_{k,\max} = 0.1$ Joule, $f_{k,\max} = 1$ GHz, $P_{k,\max} = 0.5$ W, $T = 1$ seconds, and $C_k = 500$. As expected, all methods demonstrate a linear increase in the total computation bits as the transmission bandwidth increases. Meanwhile, the proposed scheme with PE and THI exhibits a slightly lower total computation bits than the scheme without PE and THI, particularly in the case with small transmission bandwidth.

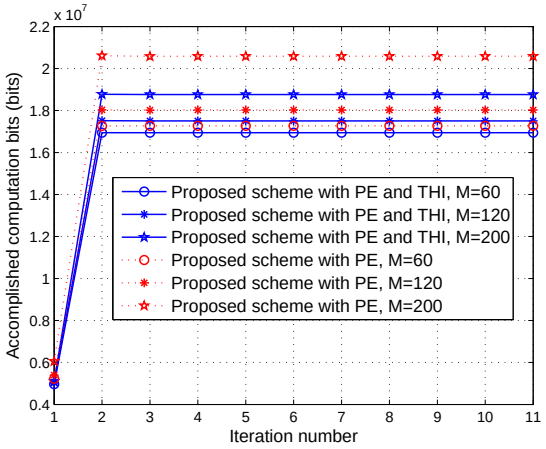

Fig. 10: Convergence of proposed algorithms.

Fig. 10 shows the convergence of proposed algorithms, where $f_{k,\max} = 1$ GHz, $E_{k,\max} = 0.1$ Joule, $P_{k,\max} = 0.5$ W, $B = 1$ MHz, $T = 1$ Seconds, and $C_k = 500$. The red lines and blue lines plot the convergence of Algorithm 2 and Algorithm 4, respectively. As observed, this simulation figure reveals that the proposed algorithms with different parameters converge to the optimal solution within several iterations. Noted that the detailed results of convergence are listed in TABLEs III-IV. This result confirms that the proposed algorithms have excellent convergence properties and low computational complexity. Additionally, it is also verified that the achievable total computation bits increases with the size of reflection elements of IRS. This reason is that a larger size of reflection units provides higher array gain to improve the task offloading rate.

VI. Conclusion

This paper investigated the computation bits maximization problem for IRS-aided MEC networks, while considering phase errors and transceiver hardware impairments. Two scenarios were studied: one with phase errors only, and another with both phase errors and transceiver hardware impairments. To acquire the optimal phase shift matrix of IRS, we transformed the stochastic phase error into a deterministic form, and utilized the successive convex approximation technique to iteratively derive the optimal phase shift of IRS in closed-form expressions. Additionally, the optimal local computing frequencies of IoT devices were derived in closed-from expressions. In the case with phase error only, we derived the optimal transmit power and time allocation in closed-form expressions by leveraging the Lagrange duality method and KKT conditions. In the case with both phase errors and transceiver hardware impairments, we used the variable substitution technique and approximation method to determine the optimal transmit power and time allocation strategy. Finally, extensive numerical results validated that the proposed method outperformed benchmark methods in terms of total accomplished computation bits, and it also verified that the phase errors and transceiver hardware impairments can cause the performance degradation of considered systems.

The current work can be extended to several interesting future works. Firstly, considering the restricted computation capability of edge servers, it is essential to design the hybrid multi-layer MEC framework to satisfy the strict computation requirements of IoT applications. Secondly, since the reflecting-only IRS can only achieve half-space coverage, it will be interesting to investigate the intelligent omni-surface-aided MEC systems, where the network resources, reflection and refraction coefficients of intelligent omni-surfaces need to be jointly designed to improve the computation performance of full-space-coverage IoT devices. Finally, the deployment location of IRS can be considered to further improve the performance of IRS-aided MEC networks.

Appendix A: Proof of *Lemma 1*

The expression of $\text{conj}(\mathbf{v}_{E,k})\mathbf{v}_{E,k}^T$ is given by

$$\begin{bmatrix} 1 & e^{j(\theta_{E,k,2}-\theta_{E,k,1})} & \dots & e^{j(\theta_{E,k,M}-\theta_{E,k,1})} \\ e^{j(\theta_{E,k,1}-\theta_{E,k,2})} & 1 & \dots & e^{j(\theta_{E,k,M}-\theta_{E,k,2})} \\ \vdots & \vdots & \ddots & \vdots \\ e^{j(\theta_{E,k,1}-\theta_{E,k,M})} & e^{j(\theta_{E,k,2}-\theta_{E,k,M})} & \dots & 1 \end{bmatrix}. \tag{42}$$

Since $\theta_{E,k,m} \sim \mathcal{U}(-\frac{\pi}{2}, \frac{\pi}{2})$, we will derive that $\Delta\theta_{i,j} = \theta_{E,k,i} - \theta_{E,k,j}$ follows the triangle distribution. Therefore, the probability density function of $\Delta\theta_{i,j}$ is expressed as

$$f_{\Delta\theta_{i,j}}(\Delta\theta) = \begin{cases} \frac{\Delta\theta}{\pi^2} + \frac{1}{\pi}, & -\pi \le \Delta\theta \le 0 \\ -\frac{\Delta\theta}{\pi^2} + \frac{1}{\pi}, & 0 < \Delta\theta \le \pi \\ 0, & \text{otherwise} \end{cases} \tag{43}$$

$\mathbb{E}_{\Delta\theta_{i,j}}(e^{j\Delta\theta_{i,j}})$ is thus calculated as

$$\begin{aligned} \mathbb{E}_{\Delta\theta_{i,j}}(e^{j\Delta\theta_{i,j}}) &= \int_{-\pi}^{0} (\frac{\Delta\theta}{\pi^2} + \frac{1}{\pi}) e^{j\Delta\theta} d\Delta\theta \\ &+ \int_{0}^{\pi} (-\frac{\Delta\theta}{\pi^2} + \frac{1}{\pi}) e^{j\Delta\theta} d\Delta\theta = \frac{4}{\pi^2}. \end{aligned} \tag{44}$$

Hence, $\mathbb{E}_{\mathbf{v}_{E,k}}(\text{conj}(\mathbf{v}_{E,k})\mathbf{v}_{E,k}^T)$ will be

$$\mathbb{E}_{\mathbf{v}_{E,k}}(\text{conj}(\mathbf{v}_{E,k})\mathbf{v}_{E,k}^T) = \begin{bmatrix} 1 & \frac{4}{\pi^2} & \dots & \frac{4}{\pi^2} \\ \frac{4}{\pi^2} & 1 & \dots & \frac{4}{\pi^2} \\ \vdots & \vdots & \ddots & \vdots \\ \frac{4}{\pi^2} & \frac{4}{\pi^2} & \dots & 1 \end{bmatrix} = \mathbf{R}. \tag{45}$$

Meanwhile, we can derive $\mathbb{E}_{\theta_{E,k,j}}(e^{j\theta_{E,k,j}})$ and $\mathbb{E}_{\theta_{E,k,j}}(e^{-j\theta_{E,k,j}})$ as

$$\mathbb{E}_{\theta_{E,k,j}}(e^{j\theta_{E,k,j}}) = \int_{-\frac{\pi}{2}}^{\frac{\pi}{2}} \frac{1}{\pi} e^{j\theta_{E,k,j}} d\theta_{E,k,j} = \frac{2}{\pi}, \tag{46}$$

TABLE III: Convergence results of Algorithm 2

Iteration number	1	2	3	4	5	6
$M = 60$	5.2245×10^6	1.7268×10^7	1.7268×10^7	1.7268×10^7	1.7268×10^7	1.7268×10^7
$M = 120$	5.3993×10^6	1.8031×10^7	1.8021×10^7	1.8022×10^7	1.8022×10^7	1.8022×10^7
$M = 200$	6.0547×10^6	2.0611×10^7	2.0576×10^7	2.0581×10^7	2.0581×10^7	2.0581×10^7

TABLE IV: Convergence results of Algorithm 4

Iteration number	1	2	3	4	5	6
$M = 60$	4.9677×10^6	1.6941×10^7	1.6941×10^7	1.6941×10^7	1.6941×10^7	1.6941×10^7
$M = 120$	5.0280×10^6	1.7513×10^7	1.7507×10^7	1.7507×10^7	1.7507×10^7	1.7507×10^7
$M = 200$	5.1107×10^6	1.8771×10^7	1.8761×10^7	1.8763×10^7	1.8763×10^7	1.8763×10^7

$$\mathbb{E}_{\theta_{E,k,j}}(e^{-j\theta_{E,k,j}}) = \int_{-\frac{\pi}{2}}^{\frac{\pi}{2}} \frac{1}{\pi} e^{-j\theta_{E,k,j}} d\theta_{E,k,j} = \frac{2}{\pi}. \quad (47)$$

Therefore, it follows that

$$\mathbb{E}_{\mathbf{v}_{E,k}}(\mathbf{v}_{E,k}^T) = [\mathbb{E}_{\theta_{E,k,1}}(e^{j\theta_{E,k,1}}), \mathbb{E}_{\theta_{E,k,2}}(e^{j\theta_{E,k,2}}), \ldots, \mathbb{E}_{\theta_{E,k,M}}(e^{j\theta_{E,k,M}})] = \frac{2}{\pi}\mathbf{1}^T. \quad (48)$$

$$\mathbb{E}_{\mathbf{v}_{E,k}}(\text{conj}(\mathbf{v}_{E,k})) = [\mathbb{E}_{\theta_{E,k,1}}(e^{-j\theta_{E,k,1}}), \mathbb{E}_{\theta_{E,k,2}}(e^{-j\theta_{E,k,2}}), \ldots, \mathbb{E}_{\theta_{E,k,M}}(e^{-j\theta_{E,k,M}})]^T = \frac{2}{\pi}\mathbf{1}. \quad (49)$$

By introducing $\mathbb{E}_{\mathbf{v}_{E,k}}(\text{conj}(\mathbf{v}_{E,k})\mathbf{v}_{E,k}^T)$, $\mathbb{E}_{\mathbf{v}_{E,k}}(\mathbf{v}_{E,k}^T)$ and $\mathbb{E}_{\mathbf{v}_{E,k}}(\text{conj}(\mathbf{v}_{E,k}))$ into $\mathbb{E}_{\mathbf{v}_{E,k}}(a_k)$, *Lemma 1* will be proved as given in (12).

REFERENCES

[1] Y. Mao, C. You, J. Zhang, K. Huang, and K. B. Letaief, "A survey on mobile edge computing: The communication perspective," *IEEE Communications Surveys and Tutorials*, vol. 19, no. 4, pp. 2322–2358, Fourth Quarter. 2017.

[2] S. Mao, J. Wu, L. Liu, D. Lan, and A. Taherkordi, "Energy-efficient cooperative communication and computation for wireless powered mobile-edge computing," *IEEE Systems Journal*, vol. 16, no. 1, pp. 287–298, 2022.

[3] Y. Yang, Y. Gong, and Y.-C. Wu, "Intelligent reflecting surface aided mobile edge computing with binary offloading: Energy minimization for IoT devices," *IEEE Internet of Things Journal*, pp. 1–1, 2022.

[4] B. Shang, H. V. Poor, and L. Liu, "Aerial reconfigurable intelligent surfaces meet mobile edge computing," *IEEE Wireless Communications*, pp. 1–9, 2022.

[5] Q. Wu and R. Zhang, "Intelligent reflecting surface enhanced wireless network via joint active and passive beamforming," *IEEE Transactions on Wireless Communications*, vol. 18, no. 11, pp. 5394–5409, Nov. 2019.

[6] C. Huang, A. Zappone, G. C. Alexandropoulos, M. Debbah, and C. Yuen, "Reconfigurable intelligent surfaces for energy efficiency in wireless communication," *IEEE Transactions on Wireless Communications*, vol. 18, no. 8, pp. 4157–4170, 2019.

[7] C. Pan, H. Ren, K. Wang, M. Elkashlan, A. Nallanathan, J. Wang, and L. Hanzo, "Intelligent reflecting surface aided mimo broadcasting for simultaneous wireless information and power transfer," *IEEE Journal on Selected Areas in Communications*, vol. 38, no. 8, pp. 1719–1734, 2020.

[8] J. Hu, H. Zhang, B. Di, L. Li, K. Bian, L. Song, Y. Li, Z. Han, and H. V. Poor, "Reconfigurable intelligent surface based RF sensing: Design, optimization, and implementation," *IEEE Journal on Selected Areas in Communications*, vol. 38, no. 11, pp. 2700–2716, 2020.

[9] B. Di, H. Zhang, L. Song, Y. Li, Z. Han, and H. V. Poor, "Hybrid beamforming for reconfigurable intelligent surface based multi-user communications: Achievable rates with limited discrete phase shifts," *IEEE Journal on Selected Areas in Communications*, vol. 38, no. 8, pp. 1809–1822, 2020.

[10] C. Pan, H. Ren, K. Wang, W. Xu, M. Elkashlan, A. Nallanathan, and L. Hanzo, "Multicell MIMO communications relying on intelligent reflecting surfaces," *IEEE Transactions on Wireless Communications*, vol. 19, no. 8, pp. 5218–5233, 2020.

[11] Z. Tang, T. Hou, Y. Liu, J. Zhang, and L. Hanzo, "Physical layer security of intelligent reflective surface aided NOMA networks," *IEEE Transactions on Vehicular Technology*, vol. 71, no. 7, pp. 7821–7834, 2022.

[12] Y. Chen, B. Ai, H. Zhang, Y. Niu, L. Song, Z. Han, and H. Vincent Poor, "Reconfigurable intelligent surface assisted device-to-device communications," *IEEE Transactions on Wireless Communications*, vol. 20, no. 5, pp. 2792–2804, 2021.

[13] M. Fu, Y. Zhou, Y. Shi, and K. B. Letaief, "Reconfigurable intelligent surface empowered downlink non-orthogonal multiple access," *IEEE Transactions on Communications*, vol. 69, no. 6, pp. 3802–3817, 2021.

[14] P. Wang, J. Fang, X. Yuan, Z. Chen, and H. Li, "Intelligent reflecting surface-assisted millimeter wave communications: Joint active and passive precoding design," *IEEE Transactions on Vehicular Technology*, vol. 69, no. 12, pp. 14 960–14 973, 2020.

[15] Y. Pan, K. Wang, C. Pan, H. Zhu, and J. Wang, "Sum-rate maximization for intelligent reflecting surface assisted terahertz communications," *IEEE Transactions on Vehicular Technology*, vol. 71, no. 3, pp. 3320–3325, 2022.

[16] Q. Wu and R. Zhang, "Joint active and passive beamforming optimization for intelligent reflecting surface assisted SWIPT under QoS constraints," *IEEE Journal on Selected Areas in Communications*, vol. 38, no. 8, pp. 1735–1748, 2020.

[17] Z. Chu, Z. Zhu, F. Zhou, M. Zhang, and N. Al-Dhahir, "Intelligent reflecting surface assisted wireless powered sensor networks for internet of things," *IEEE Transactions on Communications*, vol. 69, no. 7, pp. 4877–4889, 2021.

[18] T. Bai, C. Pan, Y. Deng, M. Elkashlan, A. Nallanathan, and L. Hanzo, "Latency minimization for intelligent reflecting surface aided mobile edge computing," *IEEE Journal on Selected Areas in Communications*, vol. 38, no. 11, pp. 2666–2682, 2020.

[19] T. Bai, C. Pan, H. Ren, Y. Deng, M. Elkashlan, and A. Nallanathan, "Resource allocation for intelligent reflecting surface aided wireless powered mobile edge computing in OFDM systems," *IEEE Transactions on Wireless Communications*, vol. 20, no. 8, pp. 5389–5407, 2021.

[20] Z. Chu, P. Xiao, M. Shojafar, D. Mi, J. Mao, and W. Hao, "Intelligent reflecting surface assisted mobile edge computing for internet of things," *IEEE Wireless Communications Letters*, vol. 10, no. 3, pp. 619–623, 2021.

[21] C. Sun, W. Ni, Z. Bu, and X. Wang, "Energy minimization for intelligent reflecting surface-assisted mobile edge computing," *IEEE Transactions on Wireless Communications*, vol. 21, no. 8, pp. 6329–6344, 2022.

[22] X. Hu, C. Masouros, and K.-K. Wong, "Reconfigurable intelligent surface aided mobile edge computing: From optimization-based to location-only learning-based solutions," *IEEE Transactions on Communications*, vol. 69, no. 6, pp. 3709–3725, 2021.

[23] Z. Li, M. Chen, Z. Yang, J. Zhao, Y. Wang, J. Shi, and C. Huang, "Energy efficient reconfigurable intelligent surface enabled mobile edge computing networks with NOMA," *IEEE Transactions on Cognitive Communications and Networking*, vol. 7, no. 2, pp. 427–440, 2021.

[24] S. Mao, L. Liu, N. Zhang, M. Dong, J. Zhao, J. Wu, and V. C. M. Leung, "Reconfigurable intelligent surface-assisted secure mobile edge computing networks," *IEEE Transactions on Vehicular Technology*, vol. 71, no. 6, pp. 6647–6660, 2022.

[25] B. Li, W. Wu, Y. Li, and W. Zhao, "Intelligent reflecting surface

and artificial-noise-assisted secure transmission of MEC system," *IEEE Internet of Things Journal*, vol. 9, no. 13, pp. 11 477–11 488, 2022.
[26] D. Li, "Ergodic capacity of intelligent reflecting surface-assisted communication systems with phase errors," *IEEE Communications Letters*, vol. 24, no. 8, pp. 1646–1650, 2020.
[27] H. Shen, W. Xu, S. Gong, C. Zhao, and D. W. K. Ng, "Beamforming optimization for IRS-aided communications with transceiver hardware impairments," *IEEE Transactions on Communications*, vol. 69, no. 2, pp. 1214–1227, 2020.
[28] M. A. Saeidi, M. J. Emadi, H. Masoumi, M. R. Mili, D. W. K. Ng, and I. Krikidis, "Weighted sum-rate maximization for multi-IRS-assisted full-duplex systems with hardware impairments," *IEEE Transactions on Cognitive Communications and Networking*, vol. 7, no. 2, pp. 466–481, 2021.
[29] G. Zhou, C. Pan, H. Ren, K. Wang, and Z. Peng, "Secure wireless communication in RIS-aided MISO system with hardware impairments," *IEEE Wireless Communications Letters*, vol. 10, no. 6, pp. 1309–1313, 2021.
[30] Z. Xing, R. Wang, J. Wu, and E. Liu, "Achievable rate analysis and phase shift optimization on intelligent reflecting surface with hardware impairments," *IEEE Transactions on Wireless Communications*, vol. 20, no. 9, pp. 5514–5530, 2021.
[31] Z. Chu, J. Zhong, P. Xiao, D. Mi, W. Hao, R. Tafazolli, and A. P. Feresidis, "RIS assisted wireless powered IoT networks with phase shift error and transceiver hardware impairment," *IEEE Transactions on Communications*, vol. 70, no. 7, pp. 4910–4924, 2022.
[32] S. Mao, L. Liu, N. Zhang, J. Hu, K. Yang, M. Dong, and K. Ota, "Resource scheduling for intelligent reflecting surface-assisted full-duplex wireless-powered communication networks with phase errors," *IEEE Internet of Things Journal*, vol. 10, no. 7, pp. 6018–6030, 2023.
[33] S. Mao, N. Zhang, L. Liu, J. Wu, M. Dong, K. Ota, T. Liu, and D. Wu, "Computation rate maximization for intelligent reflecting surface enhanced wireless powered mobile edge computing networks," *IEEE Transactions on Vehicular Technology*, vol. 70, no. 10, pp. 10 820–10 831, 2021.
[34] T. D. Burd and R. W. Brodersen, "Processor design for portable systems," *Journal of VLSI signal processing systems for signal, image and video technology*, vol. 13, no. 2-3, pp. 203–221, 1996.
[35] H. Jiang, X. Dai, Z. Xiao, and A. Iyengar, "Joint task offloading and resource allocation for energy-constrained mobile edge computing," *IEEE Transactions on Mobile Computing*, vol. 22, no. 7, pp. 4000–4015, 2023.
[36] F. Zhou, Y. Wu, R. Q. Hu, and Y. Qian, "Computation rate maximization in UAV-enabled wireless-powered mobile-edge computing systems," *IEEE Journal on Selected Areas in Communications*, vol. 36, no. 9, pp. 1927–1941, 2018.
[37] Y. Xu, H. Xie, and R. Q. Hu, "Max-min beamforming design for heterogeneous networks with hardware impairments," *IEEE Communications Letters*, vol. 25, no. 4, pp. 1328–1332, 2021.
[38] P. Wang, Z. Zheng, B. Di, and L. Song, "HetMEC: Latency-optimal task assignment and resource allocation for heterogeneous multi-layer mobile edge computing," *IEEE Transactions on Wireless Communications*, vol. 18, no. 10, pp. 4942–4956, 2019.
[39] Y. Zhang, B. Di, P. Wang, J. Lin, and L. Song, "HetMEC: Heterogeneous multi-layer mobile edge computing in the 6G era," *IEEE Transactions on Vehicular Technology*, vol. 69, no. 4, pp. 4388–4400, 2020.
[40] S. Boyd, S. P. Boyd, and L. Vandenberghe, *Convex optimization*. Cambridge university press, 2004.
[41] X. Hu, K. Wong, and K. Yang, "Wireless powered cooperation-assisted mobile edge computing," *IEEE Transactions on Wireless Communications*, vol. 17, no. 4, pp. 2375–2388, Apr. 2018.
[42] P. Chen, Y. Yang, J. Jiang, B. Lyu, Z. Yang, and A. Jamalipour, "Computational rate maximization for IRS-assisted multi-antenna WP-MEC systems with finite edge computing capability," *IEEE Internet of Things Journal*, pp. 1–1, 2023.
[43] G. Chen, Q. Wu, W. Chen, D. W. K. Ng, and L. Hanzo, "IRS-aided wireless powered MEC systems: TDMA or NOMA for computation offloading?" *IEEE Transactions on Wireless Communications*, vol. 22, no. 2, pp. 1201–1218, 2023.

Sun Mao received the Ph.D. degree in communication and information systems from the University of Electronic Science and Technology of China, Chengdu, China, in 2020. He is currently a lecturer with the College of Computer Science, Sichuan Normal University. His research interests include simultaneous wireless information and power transfer, mobile edge computing, and intelligent reflecting surface-assisted wireless communications.

Ning Zhang received the Ph.D. degree from the University of Waterloo, Canada, in 2015. He was a Post-Doctoral Research Fellow with the University of Waterloo and also with the University of Toronto, Canada. He is currently an Associate Professor with the University of Windsor, Canada. He received the Best Paper Awards from IEEE Globecom in 2014, IEEE WCSP in 2015, and the Journal of Communications and Information Networks in 2018, IEEE ICC in 2019, the IEEE Technical Committee on Transmission Access and Optical Systems in 2019, and IEEE ICCC in 2019, respectively. He also serves/served as a track chair for several international conferences and a co-chair for several international workshops. He serves as an Associate Editor for the IEEE Internet of Things Journal, the IEEE Transactions on Mobile Computing, IEEE Transactions on Cognitive Communications and Networking, IEEE Access, IET Communications, and Vehicular Communications. He was a Guest Editor of several international journals, such as the IEEE Wireless Communications, the IEEE Transactions on Industrial Informatics, and the IEEE Transactions on Cognitive Communications and Networking.

Jie Hu received his B.Eng. and M.Sc. degrees from Beijing University of Posts and Telecommunications, China, in 2008 and 2011, respectively, and received the Ph.D. degree from the School of Electronics and Computer Science, University of Southampton, U.K., in 2015. Since March 2016, he has been working with the School of Information and Communication Engineering, University of Electronic Science and Technology of China (UESTC), China. He is now a Research Professor. He has been elected into UESTCs Fundamental Research Program for Young Scientists since 2018. He also won UESTCs Academic Young Talent Award in 2019. Now he is supported by the "100 Talents" program of UESTC. His research now is mainly funded by National Natural Science Foundation of China (NSFC). He is an editor for IEEE Wireless Communications Letters, China Communications, and IET Smart Cities. He serves for IEEE Communications Magazine, IEEE/CIC China Communications, Frontiers in Communications and Networks as well as ZTE communications as a guest editor. He is a program vice-chair for IEEE TrustCom 2020 and a technical program committee (TPC) chair for IEEE UCET 2021. He also serves as a TPC member for several prestigious IEEE conferences, such as IEEE Globecom/ICC/WCSP and etc. He has won the best paper award of IEEE SustainCom 2020. His current research focuses on wireless communications and resource management for 6G, wireless information and power transfer as well as integrated communication, computing and sensing.

Kun Yang received his PhD from the Department of Electronic and Electrical Engineering of University College London (UCL), UK. He is currently a Chair Professor in the School of Computer Science and Electronic Engineering, University of Essex, UK, leading the Network Convergence Laboratory (NCL). He is also an affiliated professor of UESTC, China. His main research interests include wireless networks and communications, future Internet and edge computing. In particular he is interested in energy aspects of future communication systems such as 6G, promoting energy self-sustainability via both energy efficiency (green communications and networks) and energy harvesting (wireless charging). He has managed research projects funded by UK EPSRC, EU FP7/H2020, and industries. He has published 400+ papers and filed 30 patents. He serves on the editorial boards of a number of IEEE journals (e.g., IEEE TNSE, TVT, WCL). He is a Deputy Editor-in-Chief of IET Smart Cities Journal. He has been a Judge of GSMA GLOMO Award at World Mobile Congress Barcelona since 2019. He was a Distinguished Lecturer of IEEE ComSoc (2020-2021). He is a Member of Academia Europaea (MAE), a Fellow of IEEE, a Fellow of IET and a Distinguished Member of ACM.

Youzhi Xiong received the B.S. degree in communication engineering from the Henan University, Kaifeng, China, in 2011, the M.S. and the Ph.D degrees in electrical engineering from the University of Electronic Science and Technology of China, Chengdu, China, in 2014 and 2019, respectively. He is currently an Associate Professor with Sichuan Normal University, Chengdu, China. His research interests include massive MIMO with low resolution ADCs and/or DACs, channel estimation and data detection on massive MIMO, and reconfigurable-reflecting-surface aided communications.

Xiaosha Chen is currently working as a lecturer in College of Computer Science and Technology (College of Data Science), Taiyuan University of Technology (TYUT). He received the Ph.D. degree and bachelor's degree at the School of Information and Communication Engineering, University of Electronic Science and Technology of China (UESTC) in 2021 and 2016, respectively. His research interests include Internet of Things, performance analysis of wireless networks, network calculus and congestion control in vehicular networks.